

Optimizing over an ensemble of neural networks

Keliang Wang

Department of Operations and Information Management, School of Business, University of Connecticut

Leonardo Lozano

Operations, Business Analytics & Information Systems, University of Cincinnati

Carlos Cardonha

Department of Operations and Information Management, School of Business, University of Connecticut

David Bergman

Department of Operations and Information Management, School of Business, University of Connecticut

Abstract

We study optimization problems where the objective function is modeled through feedforward neural networks with rectified linear unit (ReLU) activation. Recent literature has explored the use of a single neural network to model either uncertain or complex elements within an objective function. However, it is well known that ensembles of neural networks produce more stable predictions and have better generalizability than models with single neural networks, which motivates the investigation of ensembles of neural networks rather than single neural networks in decision-making pipelines. We study how to incorporate a neural network ensemble as the objective function of an optimization model and explore computational approaches for the ensuing problem. We present a mixed-integer linear program based on existing popular big- M formulations for optimizing over a single neural network. We develop a two-phase approach for our model that combines preprocessing procedures to tighten bounds for critical neurons in the neural networks with a Lagrangian relaxation-based branch-and-bound approach. Experimental evaluations of our solution methods suggest that using ensembles of neural networks yields more stable and higher quality solutions, compared to single neural networks, and that our optimization algorithm outperforms (the adaption of) a state-of-the-art approach in terms of computational time and optimality gaps.

1 Introduction

Finding effective ways of embedding neural networks (NNs) within optimization problems can provide significant improvements in automated decision making. The potential for application of such a framework is already explored and discussed both in the literature and in practice:

1. *Unknown objective.* For example, suppose the revenue for a product is a function of advertising budget and cost, and is modeled through a NN trained from historical data. Identifying the optimal budget and cost requires embedding the NN in the optimization model.
2. *Non-linearity.* If a function does not admit an exact linear representation, a surrogate model for a global optimization problem can be trained from simulated inputs. This surrogate model, in the form of a NN, can then be used in a linear model, e.g., as the objective function.

Based on the generality of application, finding effective ways of handling NNs within an optimization problem opens the door for enhanced decision making capability. A major issue is

immediately realized: can we trust the output from the NN model at the solution identified by an optimizer? NNs have a tendency to produce highly variable predictions, even for minor changes in inputs, and so optimization problems where the features are variables poses significant risks.

To address the challenge of highly variable outputs from NNs, we explore in this paper the use of ensemble of NNs in optimization problems instead of single NNs (a preliminary version of this work appears in a recent conference paper (Wang et al. 2021)). It is well known that ensembles can produce competitive predictive accuracy compared to a single NN with lower variability and better generalizability (Dietterich 2000, Zhou et al. 2002), therefore suggesting that their use is particularly well suited for a decision making pipeline. However, this leads to a challenging optimization problem; optimizing over one NN can be time consuming (Anderson et al. 2020), and existing models become even more challenging when adapted to solve ensembles.

Our focus in this study is therefore to:

1. Introduce the use of NN ensemble to replace single NN within an optimization decision pipeline and demonstrate that NN ensemble can alleviate the issue of variability in predictions; and
2. Investigate algorithmic enhancements for optimization models with embedded NN ensembles.

To point 1, we evaluate the quality of the enhanced modeling paradigm (i.e., of replacing a single NN by an ensemble of NNs) by comparing the solutions identified. We show through computations on four surrogate models for global optimization benchmark functions that the solutions obtained through using an ensemble are of higher quality and more stable (i.e., the variance is lower).

To point 2, we adapt an existing big- M integer programming formulation (Fischetti and Jo 2018, Cheng et al. 2017, Anderson et al. 2020) and propose a Two Phase algorithm. The first phase combines a preprocessing procedure that seeks to strengthen the baseline formulation by finding strong bounds for variables associated with a subset of critical nodes and a set of valid inequalities derived from Benders optimality cuts for a decomposition of the problem. In the second phase we develop a Lagrangian relaxation-based branch-and-bound method. We assess the performance of our algorithms using four global optimization benchmark functions and two real-world data sets. The results exhibit a superiority of our algorithm over a benchmark state-of-the-art branch-and-cut approach in terms of computational performance.

The reminder of the paper is organized as follows. After providing a literature review in Section 2, we introduce the notation and a baseline model in Section 3. Section 4 presents our proposed Two Phase algorithm. We present the results of our experiments in Section 5 and conclude with directions for future work in Section 6.

2 Literature Review

We investigate a category of optimization problems where components of the objective function are represented (or approximated) by a Machine Learning model $\hat{f}(x; \theta)$, characterized by a vector θ of fixed parameters and a vector x of input features, whose values can be selected and optimized by the underlying optimization model. We restrict our attention to ensembles of neural networks with Rectified Linear Unit (ReLU) activation functions, which can be formulated as mixed-integer linear programs (MILP). Other predictive models that have been investigated in the optimization literature include logistic regression, linear models, decision trees, random forests, and single neural networks with ReLU activation functions (Bergman et al. 2019, Verwer et al. 2017, Biggs et al. 2017, Mišić 2020). Predictive models can be used to eschew computational intractability by serving as surrogates for complex (e.g., highly nonlinear) functions within an optimization framework (Liu et al. 2020, Bertsimas et al. 2016, Xiao et al. 2019). Nevertheless, optimizing over a predictive model can be computationally challenging; for example, maximizing (or minimizing) the output of random forests or neural networks is NP-hard (Mišić 2020, Katz et al. 2017).

Recent studies on solving optimization models with embedded neural networks have explored different techniques to encode neural networks. [Schweidtmann and Mitsos \(2019\)](#) study neural networks with hyperbolic tangent (`tanh`) activation functions to solve deterministic global optimization problems; the formulation is solved by a customized branch-and-bound based solver that relies on McCormick relaxations of the `tanh` activation functions. [Bartolini et al. \(2011\)](#) propose so-called neuron constraints to incorporate NN formulations into a constraint programming approach ([Bartolini et al. 2011](#)). Recent work has focused mainly on neural networks with ReLU activation functions, in part because (1) the ReLU function is recommended as a default activation when training neural networks, as it performs well in numerous applications ([Goodfellow et al. 2016](#)); and (2) the piecewise linear nature of ReLU admits a relatively simple big- M formulation that is easily incorporated within MILP models.

A recent line of research concentrates on using MILPs to verify certain properties of neural networks, including reachability analysis of NNs ([Lomuscio and Maganti 2017](#)), robustness of NNs to adversarial inputs ([Cheng et al. 2017](#), [Tjeng et al. 2019](#), [Xiao et al. 2019](#), [Fischetti and Jo 2018](#)), and output range of a trained NN ([Dutta et al. 2018](#)); the formulations used in these articles are expressed essentially as MILPs (see also [Bunel et al. \(2018\)](#), [Botoeva et al. \(2020\)](#)). More recently, MILPs have also been used for reducing the size of trained neural networks ([Serra et al. \(2020\)](#)) and finding the expressiveness of NNs ([Serra et al. 2018](#)).

Furthermore, different techniques have been explored to speed up the solution times for NN-embedded optimization models. As the constant values used in big- M formulations affect the strength of a problem formulation and, consequently, its solution time ([Vielma 2015](#)), several pre-processing procedures have been proposed to identify tighter bounds for the big- M values ([Cheng et al. 2017](#), [Dutta et al. 2018](#), [Tjeng et al. 2019](#), [Fischetti and Jo 2018](#), [Grimstad and Andersson 2019](#)); we discuss these methods in Section 4, as they are closely related to our proposed techniques. [Lombardi and Gualandi \(2016\)](#) apply Lagrangian relaxation to a NN with one hidden layer and `tanh` as activation function, and use the subgradient method to optimize for tighter bounds. [Bunel et al. \(2018\)](#) split the input domain to form smaller MILPs restricted to each part of the solution space. [Botoeva et al. \(2020\)](#) define dependency relations between neurons in terms of their activation (or deactivation) and explore them to derive cuts that reduce the search space. [Anderson et al. \(2020\)](#) propose an exponentially-sized convex hull formulation for a single neuron and provide an efficient separation procedure to find the most violated inequality at any given fractional point. [Tsay et al. \(2021\)](#) extend the work of [Anderson et al. \(2020\)](#) by partitioning the input vector of a ReLU function into groups and considering convex hull formulations over the partitions via disjunctive programming. Depending on the number of partitions, their formulation is able to approximate the convex hull of a ReLU function with fewer number of constraints and auxiliary variables than the ideal formulation of [Anderson et al. \(2020\)](#).

Predictive models are typically not exact mappings. Therefore, there may exist discrepancies between the predicted and the actual value of a feasible solution, so predict-and-optimize models may incorrectly prove the optimality of sub-optimal solutions (see e.g., [Smith and Winkler \(2006\)](#)). The inaccuracy of predictive models tends to increase in regions of the solution space that are not adequately covered by the samples in the training set, so one mitigation strategy consists of restricting the feasibility of the optimization problem to well-populated regions of the solution space, i.e., feasible solutions must be close to the existing data points ([Biggs et al. 2017](#), [Bertsimas and Kallus 2020](#), [Maragno et al. 2021](#), [Wasserkrug et al. 2022](#)). This distance-based condition can be enforced either through the incorporation of constraints ([Thebelt et al. 2021](#), [Shi et al. 2022](#)) or as a penalty term in the objective function ([Mistry et al. 2021](#)). Distance measures used in the area include the Euclidean and Manhattan distances ([Thebelt et al. 2021](#)), as well as the Mahalanobis distance and the average distance from the nearest neighbour points ([Shi et al. 2022](#)). Another strategy consists of restricting the feasible region to the convex hull of the training set (see e.g., [Biggs et al. \(2017\)](#), [Maragno et al. \(2021\)](#)).

Our work focuses on solution methods for ensembles of neural networks. [Dietterich \(2000\)](#) provides statistical, computational and representational arguments to show that an ensemble is always able to outperform each of its individual component estimators. Ensembles of neural

network were introduced by Hansen and Salamon (1990) and have gained substantial development over the last years (see Li et al. (2018) for a detailed survey). The idea of exploring NNs as proxies for complex models have been explored in the online learning setting by Lu and Van Roy (2017); the authors use ensembles to develop an adaptation of Thompson sampling to scenarios where the underlying models are intractable. To the best of our knowledge, our work is the first to consider ensembles of NNs for offline optimization.

The literature is rich in examples where the integration of predictive models and optimization has been successfully applied to real-world problems. Bertsimas et al. (2016) optimize over a ridge regression model to recommend effective treatments for cancer. Liu et al. (2020) use linear estimators of travel times to optimize real-time order assignments for a food service provider. Other examples can be found in scholarship allocation for admitted students to maximize class size (Bergman et al. 2019), personalized pricing to maximize revenue (Biggs et al. 2021), and ordering of the items to sell in an auction to maximize expected revenue (Verwer et al. 2017). The growing interest in the area has fostered the development of several software packages that facilitate the development of models based on the integration of optimization and machine learning; some examples are Lombardi et al. (2017), Bergman et al. (2019), Maragno et al. (2021), and Thebelt et al. (2021).

3 Basic Optimization Model

The problem we study is as follows. Given a function f , let $\mathcal{E}_f = \{N^1, N^2, \dots, N^e\}$ be an ensemble of e NNs representing f and Ω be the feasible set of possible inputs to the ensemble. In general, an ensemble is built in two steps: a method to train multiple estimators and the approach to combine their predictions. We adopt the popular Bagging method (Breiman 1996) for training NNs and use the averaging method to combine predictions. An estimate of f for any point x in Ω produced by \mathcal{E}_f is given by the average of the individual estimates of each neural network in \mathcal{E}_f , that is,

$$\mathcal{E}_f(x) = \frac{1}{e} \sum_{i=1}^e N^i(x).$$

We study the following problem:

$$\max_{x \in \Omega} \mathcal{E}_f(x) \tag{1}$$

We now present our baseline optimization model, which was first proposed in Wang et al. (2021) and is a straightforward extension of existing MIP models for optimizing over a single NN (see e.g., Fischetti and Jo (2018)). Consider an ensemble $\mathcal{N} \equiv \{N_1, \dots, N_e\}$ of e neural networks. Each NN is a layered graph and we refer to each vertex in a NN as a neuron. Let L_i denote the number of layers and n_l^i denote the number of neurons in the l -th layer of N_i , $i \in \{1, \dots, e\}$. We use vector $(n_1^i, \dots, n_{L_i}^i)$ to succinctly represent the architecture of N_i and assume that $n_{L_i}^i = 1$ for all $i \in \{1, \dots, e\}$, i.e., there is only one neuron in the output layer of each NN in \mathcal{N} . We refer to $\{2, 3, \dots, L_i - 1\}$ as the set of intermediate layers of N_i , i.e., all layers except the first and the last. Finally, the neural networks of \mathcal{N} do not share neurons or arcs, so the description of each neural network N_i of \mathcal{N} , described next, provides a complete characterization of the ensemble.

Let $v_j^{i,l}$ denote the j^{th} neuron in layer l of N_i . Each $v_j^{i,l}$ receives a series of inputs and produces a single (scalar) output $y_j^{i,l}$. For the j -th neuron of the first layer, both its input and its output is the j -th coordinate of x , i.e., $v_j^{i,1}$ receives x_j , the j^{th} component of the decision variables vector, and returns

$$y_j^{i,1} = x_j.$$

Observe that all NNs of an ensemble \mathcal{N} must have the same number of nodes in the first layer, so we occasionally simplify the notation by dropping the reference to the NN and use n_1 instead of n_1^i .

Each neuron $v_j^{i,l}$ of an intermediate layer l receives a vector of inputs $\mathbf{y}^{i,l-1} \equiv [y_1^{i,l-1}, \dots, y_{n_{l-1}}^{i,l-1}]$, given by the outputs of the neurons in the previous layer. The output $y_j^{i,l}$ of $v_j^{i,l}$ is defined as

$$y_j^{i,l} = \text{ReLU}\left((\mathbf{W}_j^{i,l})^\top \mathbf{y}^{i,l-1} + b_j^{i,l}\right), \quad (2)$$

where $\text{ReLU} : \mathbb{R} \rightarrow \mathbb{R}^+$ is the Rectified Linear Unit (ReLU) activation function, defined as $\text{ReLU}(\bullet) \equiv \max(0, \bullet)$. $\mathbf{W}_j^{i,l} \in \mathbb{R}^{n_{l-1}}$ is a *weight* vector and $b_j^{i,l} \in \mathbb{R}$ is a *bias* scalar. Both $\mathbf{W}_j^{i,l}$ and $b_j^{i,l}$ are generated during the training process of N_i and, for the purpose of optimization over \mathcal{N} , they are fixed (i.e., these values cannot be modified).

Finally, the output y_1^{i,L_i} of v_1^{i,L_i} , the single terminal neuron in the last layer of N_i , is computed as an affine combination of the previous layer's output without applying the ReLU function, i.e.,

$$y_1^{i,L_i} = (\mathbf{W}_1^{i,L_i})^\top \mathbf{y}^{i,L_i-1} + b_1^{i,L_i}.$$

3.1 Formulation of ReLU functions

The fundamental building block of our formulation is a mathematical programming representation of the ReLU function for a single neuron, which has been widely used in the literature (Fischetti and Jo 2018, Tjeng et al. 2019, Anderson et al. 2020). For each neuron $v_j^{i,l}$, we define an auxiliary continuous variable $h_j^{i,l}$ to capture the linear component of Expression 2, which is the value of the affine combination of the neuron's inputs before applying the ReLU function (also known as the *pre-activation*). Additionally, we define a binary variable $z_j^{i,l}$ that takes a value of 1 if $v_j^{i,l}$ is *active* (i.e., its output is strictly greater than 0). Finally, assume that a lower bound $\text{LB}_j^{i,l} < 0$ and upper bound $\text{UB}_j^{i,l} > 0$ are known for each $h_j^{i,l}$, i.e., $h_j^{i,l} \in [\text{LB}_j^{i,l}, \text{UB}_j^{i,l}]$; observe that neurons for which both bounds are either non-positive or non-negative can be removed or merged (Serra et al. 2020). A MILP formulation that models the behaviour of $v_j^{i,l}$ is given by:

$$h_j^{i,l} = (\mathbf{W}_j^{i,l})^\top \mathbf{y}^{i,l-1} + b_j^{i,l} \quad (3a)$$

$$h_j^{i,l} \leq y_j^{i,l} \leq h_j^{i,l} - \text{LB}_j^{i,l}(1 - z_j^{i,l}) \quad (3b)$$

$$0 \leq y_j^{i,l} \leq \text{UB}_j^{i,l} z_j^{i,l} \quad (3c)$$

$$z_j^{i,l} \in \{0, 1\} \quad (3d)$$

$$h_j^{i,l}, y_j^{i,l} \in \mathbb{R} \quad (3e)$$

Constraint (3a) sets the value of $h_j^{i,l}$. Constraints (3b)–(3c) ensure that if $h_j^{i,l} > 0$, then $y_j^{i,l} = h_j^{i,l}$ and $z_j^{i,l} = 1$, i.e., they enforce that the output equals the evaluation of the ReLU function.

Observe that $\text{LB}_j^{i,l}$ and $\text{UB}_j^{i,l}$ act as big- M constants in (3b) and (3c), respectively. Therefore, the strength of Formulation (3) for $v_j^{i,l}$ strongly depends on the values of $\text{LB}_j^{i,l}$ and $\text{UB}_j^{i,l}$. One of the main contributions of this work is a strategy to compute tighter bounds, which we present in §4.1.1.

3.2 MILP formulation for optimization over ensembles

We now present an MILP formulation for optimizing over a given ensemble \mathcal{N} , which is a straightforward adaptation of Model (3) over the complete set of neurons in \mathcal{N} .

$$\max \quad \frac{1}{e} \sum_{i=1}^e y_1^{i,L_i} \quad (4a)$$

$$\text{s.t. } y_j^{i,1} = x_j \quad \forall i \in \{1, \dots, e\}, j \in \{1, \dots, n_1\} \quad (4b)$$

$$y_1^{i,L_i} = h_1^{i,L_i} \quad \forall i \in \{1, \dots, e\} \quad (4c)$$

$$h_j^{i,l} = (\mathbf{W}_j^{i,l})^\top \mathbf{y}^{i,l-1} + b_j^{i,l} \quad \forall i \in \{1, \dots, e\}, l \in \{2, \dots, L_i\}, j \in \{1, \dots, n_l^i\} \quad (4d)$$

$$h_j^{i,l} \leq y_j^{i,l} \leq h_j^{i,l} - \text{LB}_j^{i,l}(1 - z_j^{i,l}) \quad \forall i \in \{1, \dots, e\}, l \in \{2, \dots, L_i - 1\}, j \in \{1, \dots, n_l^i\} \quad (4e)$$

$$0 \leq y_j^{i,l} \leq \text{UB}_j^{i,l} z_j^{i,l} \quad \forall i \in \{1, \dots, e\}, l \in \{2, \dots, L_i - 1\}, j \in \{1, \dots, n_l^i\} \quad (4f)$$

$$z_j^{i,l} \in \{0, 1\} \quad \forall i \in \{1, \dots, e\}, l \in \{2, \dots, L_i - 1\}, j \in \{1, \dots, n_l^i\} \quad (4g)$$

$$h_j^{i,l}, y_j^{i,l} \in \mathbb{R} \quad \forall i \in \{1, \dots, e\}, l \in \{1, \dots, L_i\}, j \in \{1, \dots, n_l^i\} \quad (4h)$$

$$x \in \Omega \quad (4i)$$

Variable x corresponds to the input vector, which belongs to the (potentially constrained) set $\Omega \subseteq \mathbb{R}^{n_1}$. The objective function optimizes the average output of the last neuron in each NN. Constraints (4b) ensure that the outputs for neurons in the first layer of any NN correspond to x . Constraints (4c) set the output of the single neuron in the last layer of each NN to the affine combination of the neuron's inputs, without applying the ReLU function. Constraints (4d)–(4h) replicate Formulation (3) for each intermediate neuron in the ensemble.

3.3 Baseline algorithm

Anderson et al. (2020) investigate Formulation (3) and provide an ideal convex hull formulation in the space of the original variables with an exponential number of constraints; they propose a branch-and-cut algorithm (B&C) which iteratively finds and adds the most violated constraints at fractional solutions obtained during the exploration of the branch-and-bound tree. To the best of our knowledge, B&C is the state-of-the-art approach for optimizing over a single neural network.

As Formulation (4) is also based on Formulation (3), B&C can be directly adapted to solve our problem. As a result, we use B&C as a baseline benchmark algorithm to compare against and measure the effects of our proposed acceleration techniques in §5.

4 Two Phase Algorithm

We propose E-NN, a Two Phase algorithm, to optimize over ensemble of neural networks. The first phase relies on acceleration strategies to enhance the formulation of each NN composing the ensemble, whereas the second phase explores a Lagrangian decomposition of Formulation (4). E-NN is summarized in Algorithm 1.

Algorithm 1 Two Phase Algorithm (E-NN)

- 1: **Pre-Processing:** Compute $\text{LB}_j^{i,l}$ and $\text{UB}_j^{i,l}$ using Algorithm 2.
 - 2: **Phase One:** Execute Formulation (4) enhanced with Inequalities (10) until an optimal solution is found or a time limit is reached. Record the best feasible solution found as $(\bar{x}, \bar{y}, \bar{h}, \bar{z})$. If $(\bar{x}, \bar{y}, \bar{h}, \bar{z})$ is not proven optimal, go to Step 3; otherwise, terminate execution.
 - 3: **Phase Two:** Compute the values for Lagrangian multipliers λ by applying Q iterations of a subgradient algorithm. Execute the Lagrangian relaxation-based branch-and-bound approach until an optimal solution is found or a pre-defined time limit is reached.
-

4.1 Pre-Processing and Phase One

In the Pre-Processing stage of Algorithm 1, we use the procedure described in 4.1.1 to compute strong bounds for the nodes. We then try to solve the problem to optimality using Formulation (4) enhanced with valid inequalities (10), presented in 4.1.2. If we find an optimal solution within a phase-one time limit, then we terminate the algorithm and report an optimal solution. These techniques do not require (or explore) the fact that we have an ensemble, i.e., they handle each NN individually; consequently, the strategies presented in 4.1 can also be applied to single NNs.

4.1.1 Targeted Strong Bounds

Depending on the tightness of the bounds, the output for intermediate neurons computed at fractional solutions can greatly deviate from the correct evaluation of the ReLU function in Formulation (3). We motivate the need for strong values of $\text{LB}_j^{i,l}$ and $\text{UB}_j^{i,l}$ with an example.

Example 1. Let $v_j^{i,l}$ be a neuron of an intermediate layer with $h_j^{i,l} \in [-20, 10]$. Consider the vector $(\bar{h}_j^{i,l}, \bar{y}_j^{i,l}, \bar{z}_j^{i,l})$ of values associated with $v_j^{i,l}$ composing a fractional solution to Model (3). Because the bounds are loose, the vector $(\bar{h}_j^{i,l}, \bar{y}_j^{i,l}, \bar{z}_j^{i,l}) = (-5, 5, 0.5)$ satisfies constraints (3b) and (3c), as

$$-5 \leq 5 \leq -5 + |-20|(1 - 0.5) \quad \text{and} \quad 0 \leq 5 \leq 10(0.5),$$

respectively. Observe that the correct evaluation of the ReLU function applied to $\bar{h}_j^{i,l} = -5$ is 0 (instead of 5). Conversely, if the bounds of $h_j^{i,l}$ were tightened to $[-5, 10]$, then the same assignment $\bar{h}_j^{i,l} = -5$ could only compose a feasible solution with $\bar{y}_j^{i,l} = \bar{z}_j^{i,l} = 0$, thus yielding the correct value of $\text{ReLU}(\bar{h}_j^{i,l})$. ■

A basic procedure for computing bounds from the literature is via interval arithmetic (Cheng et al. 2017, Tjeng et al. 2019, Anderson et al. 2020). In this technique, bounds are lexicographically computed layer by layer as:

$$\text{LB}_j^{i,l} = \sum_{k \in \{1, \dots, n_{l-1}^i\}} \left(\text{LB}_k^{i,l-1} \max\{0, w_{j,k}^{i,l}\} + \text{UB}_k^{i,l-1} \min\{0, w_{j,k}^{i,l}\} \right) + b_j^{i,l}; \quad \text{and} \quad (5)$$

$$\text{UB}_j^{i,l} = \sum_{k \in \{1, \dots, n_{l-1}^i\}} \left(\text{UB}_k^{i,l-1} \max\{0, w_{j,k}^{i,l}\} + \text{LB}_k^{i,l-1} \min\{0, w_{j,k}^{i,l}\} \right) + b_j^{i,l}, \quad (6)$$

where $w_{j,k}^{i,l}$ denotes the scalar value at the k^{th} position of weight vector $\mathbf{W}_j^{i,l}$ and the bounds for neurons in the first layer are equal to the respective bounds for x . Interval arithmetic typically produces weak bounds, as over-estimated bounds from one layer are used in the computation of the bounds for the next layer, thus propagating errors through the network (Tjeng et al. 2019, Tsay et al. 2021). As an alternative to interval arithmetic, Tjeng et al. (2019) propose a *progressive bounds tightening* procedure that solves up to two linear programs for each neuron $v_j^{i,l}$.

These LPs are obtained by relaxing the integrality constraints on the z -variables and considering the objectives of maximizing and minimizing $h_j^{i,l}$. To obtain even tighter bounds, Fischetti and Jo (2018) solve two MILPs per neuron, obtained by considering the objectives of maximizing and minimizing $h_j^{i,l}$ for each critical neuron without relaxing the integrality constraints on the z -variables.

The bounding procedures described above offer a trade-off between the computational time required to compute the bounds and the quality of the bounds obtained. Interval arithmetic is quite efficient but provides weak bounds. On the other hand, solving two MILPs per neuron provide strong bounds at the expense of considerably higher computation times. In order to offset the high computational times required to obtain strong bounds, we propose solving two MIPs only for *critical neurons*, which are neurons that are likely to correspond to fractional solutions for which the ReLU function evaluation is vastly overestimated. For the non-critical neurons we compute bounds by solving two LPs as done by Tjeng et al. (2019) and Tsay et al. (2021).

The cornerstone of our proposed bounding approach is a procedure to identify such critical neurons efficiently. We start with a version of Formulation (4) that uses bounds obtained via LPs for all neurons in the neural network. After solving K nodes of the branch-and-bound tree, we identify critical neurons by *surveying* these nodes. Namely, for each fractional solution explored, denoted by $(\bar{x}, \bar{h}, \bar{y}, \bar{z})$, we record the *discrepancy* of each neuron at a given fractional solution as

$$\delta_j^{i,l}(\bar{h}, \bar{y}) = \begin{cases} \bar{y}_j^{i,l} & \text{if } \bar{h}_j^{i,l} < 0; \\ \bar{y}_j^{i,l} - \bar{h}_j^{i,l} & \text{if } \bar{h}_j^{i,l} \geq 0, \end{cases} \quad (7)$$

which captures the magnitude of the overestimation of the ReLU function by $(\bar{x}, \bar{h}, \bar{y}, \bar{z})$; observe that the correct evaluation of the ReLU function is 0 in the first case and $\bar{h}_j^{i,l}$ in the second case. A neuron is critical if its total discrepancy, given by the sum of all discrepancies computed for each of the K surveyed nodes, is greater than or equal to a given threshold τ .

After identifying the critical nodes, we identify their bounds by solving the two MILPs described above, which incorporate the integrality constraints on the z -variables and minimize and maximize $h_j^{i,l}$, respectively. Observe that, to compute the bounds for a neuron $v_j^{i,l}$, we only need to incorporate the nodes of the first $l - 1$ layers (plus $v_j^{i,l}$) in the associated MILP, so the problem is easier than the original problem. Nevertheless, solving these sub-problems can be time-consuming, so we use the best bound obtained within a time limit as an over-approximated (yet valid) substitute for the optimal objective value (as done by Fischetti and Jo (2018)). In our computational experiments we find that the best bounds from the interrupted MILPs obtained within 5 seconds are considerably tighter than the solutions from the LPs. Algorithm 2 summarizes our procedure.

Algorithm 2 Targeted Strong Bounds Procedure

- 1: Solve two LPs for each neuron to initialize the lower and upper bounds for each neuron.
- 2: Generate Formulation (4) using the LP bounds and execute the branch-and-bound algorithm until K nodes are solved.
- 3: Survey the K nodes and compute the discrepancies $\delta_j^{i,l}(\bar{h}, \bar{y})$ for each neuron $v_j^{i,l}$ at every fractional solution identified when solving Formulation (4) with the LP bounds.
- 4: Identify the set of critical neurons as

$$C = \left\{ v_j^{i,l} \mid \frac{\sum_{k=1}^K \delta_j^{i,l}(\bar{h}^k, \bar{y}^k)}{K} \geq \tau, i \in \{1, \dots, e\}, l \in \{1, \dots, L_i\}, j \in \{1, \dots, n_l^i\} \right\}.$$

- 5: Solve two MILPs for the critical neurons and use best bounds identified within the time limit.
-

After computing the strengthened bounds via Algorithm 2, we solve Formulation (4) using the updated bounds. From this procedure, it often happens that several neurons can be removed, as one can infer that they are always active (when both bounds are non-negative) or they are always inactive (when both bounds are non-positive) (Cheng et al. 2017, Serra et al. 2020).

4.1.2 Valid Inequalities

We propose a set of valid inequalities for Formulation (4) that can be interpreted as optimality Bender’s cuts (Benders 1962). Let \mathcal{Z} be the discrete space defined by the integrality constraints (4g), and let $\mathcal{X}(z)$ be the space defined by the remaining constraints (4b)–(4f) and (4h)–(4i) for a fixed binary vector z . We rewrite Formulation (4) as

$$v^* = \max_{z \in \mathcal{Z}} \max_{(x,h,y) \in \mathcal{X}(z)} \frac{1}{e} \sum_{i=1}^e y_1^{i,L_i}, \quad (8)$$

where the outer (maximization) problem contains all the binary variables and the inner (minimization) problem is a LP parameterized by the discrete decisions of the outer problem. Because of strong duality, we can modify (8) by replacing the inner maximization problem with its dual minimization problem. Let $\pi_j^{i,l}$, $\alpha_j^{i,l}$, and $\beta_j^{i,l}$ denote the dual variables associated with constraints (4d), (4e), and (4f), respectively. Let Ψ be the dual feasible space (projecting out dual variables with an objective coefficient equal to 0) and note that the dual feasible space is not parameterized by z , i.e., the set of feasible dual points remains the same independently of the discrete decisions from the outer problem. By replacing the inner problem by its dual, we can rewrite (8) as

$$v^* = \max_{z \in \mathcal{Z}} \min_{(\pi, \alpha, \beta) \in \Psi} \sum_{i=1}^e \sum_{l=2}^{L_i} \sum_{j=1}^{n_l^i} b_j^{i,l} \pi_j^{i,l} + \sum_{i=1}^e \sum_{l=2}^{L_i-1} \sum_{j=1}^{n_l^i} |\text{LB}_j^{i,l}| (1 - z_j^{i,l}) \alpha_j^{i,l} + \sum_{i=1}^e \sum_{l=2}^{L_i-1} \sum_{j=1}^{n_l^i} \text{UB}_j^{i,l} z_j^{i,l} \beta_j^{i,l}, \quad (9)$$

where the dual objective function is parameterized by the discrete decision variables z .

Proposition 1. *For any feasible dual solution $(\bar{\pi}, \bar{\alpha}, \bar{\beta}) \in \Psi$, the following inequality is valid to Formulation (4):*

$$\frac{1}{e} \sum_{i=1}^e y_1^{i,L_i} \leq \sum_{i=1}^e \sum_{l=2}^{L_i} \sum_{j=1}^{n_l^i} b_j^{i,l} \bar{\pi}_j^{i,l} + \sum_{i=1}^e \sum_{l=2}^{L_i-1} \sum_{j=1}^{n_l^i} |\text{LB}_j^{i,l}| (1 - \bar{z}_j^{i,l}) \bar{\alpha}_j^{i,l} + \sum_{i=1}^e \sum_{l=2}^{L_i-1} \sum_{j=1}^{n_l^i} \text{UB}_j^{i,l} \bar{z}_j^{i,l} \bar{\beta}_j^{i,l} \quad (10)$$

Proof. For any $\bar{z} \in \mathcal{Z}$ for which $\mathcal{X}(\bar{z}) \neq \emptyset$ define

$$v(\bar{z}) = \max_{(x,h,y) \in \mathcal{X}(\bar{z})} \frac{1}{e} \sum_{i=1}^e y_1^{i,L_i}, \quad (11)$$

and note that for any feasible primal solution $(\bar{x}, \bar{h}, \bar{y}) \in \mathcal{X}(\bar{z})$ it holds that

$$\frac{1}{e} \sum_{i=1}^e \bar{y}_1^{i,L_i} \leq v(\bar{z}). \quad (12)$$

Because of strong duality, there exists a dual solution $(\pi^*, \alpha^*, \beta^*) \in \Psi$ for which

$$v(\bar{z}) = \sum_{i=1}^e \sum_{l=2}^{L_i} \sum_{j=1}^{n_l^i} b_j^{i,l} \pi_j^{*,i,l} + \sum_{i=1}^e \sum_{l=2}^{L_i-1} \sum_{j=1}^{n_l^i} |\text{LB}_j^{i,l}| (1 - \bar{z}_j^{i,l}) \alpha_j^{*,i,l} + \sum_{i=1}^e \sum_{l=2}^{L_i-1} \sum_{j=1}^{n_l^i} \text{UB}_j^{i,l} \bar{z}_j^{i,l} \beta_j^{*,i,l}. \quad (13)$$

Because of weak duality we obtain that

$$v(\bar{z}) \leq \sum_{i=1}^e \sum_{l=2}^{L_i} \sum_{j=1}^{n_l^i} b_j^{i,l} \bar{\pi}_j^{i,l} + \sum_{i=1}^e \sum_{l=2}^{L_i-1} \sum_{j=1}^{n_l^i} |\text{LB}_j^{i,l}| (1 - \bar{z}_j^{i,l}) \bar{\alpha}_j^{i,l} + \sum_{i=1}^e \sum_{l=2}^{L_i-1} \sum_{j=1}^{n_l^i} \text{UB}_j^{i,l} \bar{z}_j^{i,l} \bar{\beta}_j^{i,l}, \quad (14)$$

for any $(\bar{\pi}, \bar{\alpha}, \bar{\beta}) \in \Psi$. This concludes the proof. ■

There exists an exponential number of valid inequalities (10). Therefore, we propose an iterative approach, where these inequalities are identified and added every time that a feasible integer solution is explored. Observe that the strength of the valid inequalities is again dependent on the quality of the lower and upper bounds.

4.2 Phase Two

If Algorithm 1 does not obtain an optimal solution at the end of Phase One, it stores the best feasible solution $(\bar{x}, \bar{y}, \bar{h}, \bar{z})$ found so far and proceeds to a second phase, in which E-NN solves Formulation (4) using a Lagrangian relaxation-based reformulation. In contrast with the Pre-Processing stage and Phase One, Phase Two applies only to ensembles with two or more NNs.

4.2.1 Lagrangian Relaxation-Based Decomposition

We propose a decomposition approach that is based on the following reformulation of Model (4):

$$\max \quad \frac{1}{e} \sum_{i=1}^e y_1^{i, L_i} \quad (15a)$$

$$\text{s.t.} \quad x_j^1 = x_j^i \quad \forall i \in \{2, \dots, e\}, j \in \{1, \dots, n_1\} \quad (15b)$$

$$y_j^{i,1} = x_j^i \quad \forall i \in \{1, \dots, e\}, j \in \{1, \dots, n_1\} \quad (15c)$$

$$(4c) - (4h) \quad (15d)$$

$$x^i \in \Omega \quad \forall i \in \{1, \dots, e\}. \quad (15e)$$

Model (15) includes one copy of the input variables for each NN in the ensemble. Constraints (15b) ensure that the j -th input variable to the i -th NN, $i \in \{2, \dots, e\}$ is equal to x_j^1 , the j -th input to N_1 ; in words, these constraints force all the NNs of the ensemble to receive the same input; observe that Models (4) and (15) are equivalent. We obtain a Lagrangian relaxation of Model (15) by moving constraints (15b) to the objective function. The resulting formulation is as follows:

$$\max \quad \frac{1}{e} \sum_{i=1}^e y_1^{i, L_i} + \sum_{i=2}^e \sum_{j=1}^{n_1} \lambda_{ij} (x_j^1 - x_j^i) \quad (16a)$$

$$\text{s.t.} \quad y_j^{i,1} = x_j^i \quad \forall i \in \{1, \dots, e\}, j \in \{1, \dots, n_1\} \quad (16b)$$

$$(4c) - (4h) \quad (16c)$$

$$x^i \in \Omega \quad \forall i \in \{1, \dots, e\}. \quad (16d)$$

Formulation (16) yields a valid upper bound on the optimal objective function of (4) for any given value of the Lagrangian multipliers λ . Formulation (16) is computationally easier to solve than (4), as the objective function (16a) is the only place in which the NNs of the ensemble interact. On the downside, there could be “disagreements” between the x -variables corresponding to different NNs in an optimal solution to (16), so the solutions identified by (16) associated with each NN may be suboptimal to (4). We address this issue by embedding (16) into a branch-and-bound approach.

4.2.2 Branching strategy

We propose a branching procedure on the input variables x , with decisions guided by the degree of disagreement between the copies of the input variables. At the root node of our branch-and-bound tree, we solve Formulation (16) allowing all input variables across all NNs of the

ensemble to assume any value in its original domains, that is,

$$x_j^i \in [\mathbf{lb}_j, \mathbf{ub}_j] \quad \forall i \in \{1, \dots, e\}, j \in \{1, \dots, n_1\}. \quad (17)$$

The values for \mathbf{lb}_j and \mathbf{ub}_j are derived from the constraints in Ω if not readily available.

Our proposed branching scheme works as follows. Consider any given node of the branch-and-bound tree in which the x -variables take values $\hat{x}_j^i \in [\hat{\mathbf{lb}}_j, \hat{\mathbf{ub}}_j]$, where $\hat{\mathbf{lb}}_j$ and $\hat{\mathbf{ub}}_j$ are the lower and upper bounds for x_j at the given node, respectively. Before branching, we first check if the local domain of the x -variables is already “small”, i.e., we check if

$$\hat{\mathbf{ub}}_j - \hat{\mathbf{lb}}_j \leq \Delta \quad \forall j \in \{1, \dots, n_1\}, \quad (18)$$

where Δ is a sufficiently small constant parameter of the algorithm. If (18) is true, then we stop branching and complete the exploration of the current node by reverting to the big-M formulation (4) subject to the domain constraints associated with the node, i.e., with Ω enriched by

$$x_j \in [\hat{\mathbf{lb}}_j, \hat{\mathbf{ub}}_j] \quad \forall j \in \{1, \dots, n_1\}$$

Otherwise, if the domains of the input variables are still “large”, we select the branching variable by first computing the maximum and minimum values of the \hat{x} -variables as:

$$x_j^{\max} = \max_{i \in \{1, \dots, e\}} \{\hat{x}_j^i\}, \quad \forall j \in \{1, \dots, n_1\} \quad \text{and} \quad x_j^{\min} = \min_{i \in \{1, \dots, e\}} \{\hat{x}_j^i\}, \quad \forall j \in \{1, \dots, n_1\}$$

and then selecting the branching variable index \hat{j} given by

$$\hat{j} = \operatorname{argmax}_{j \in \{1, \dots, n_1\}} \{x_j^{\max} - x_j^{\min}\}.$$

Note that \hat{j} is the index for which there is maximum disagreement between the copies of the input variables corresponding to different NNs. Once \hat{j} is identified, we create two branches. In the left branch we add a new child node with the updated domains given by:

$$x_j \in [\hat{\mathbf{lb}}_j, (x_j^{\max} + x_j^{\min})/2] \quad \forall j \in \{1, \dots, n_1\},$$

while in the right branch we add a new child node with the updated domains given by:

$$x_j \in [(x_j^{\max} + x_j^{\min})/2, \hat{\mathbf{ub}}_j] \quad \forall j \in \{1, \dots, n_1\}$$

As it is usually done in branch-and-bound approaches, we define a primal heuristic to obtain feasible solutions (and, in turn, lower bounds on the optimal value) faster. In our approach, we call our primal heuristic every time we solve a branch-and-bound node. Again, let the values of the x -variables at a given node be \hat{x}_j^i . Our primal heuristic simply runs the original big-M formulation (4) for N_1 , the first NN of the ensemble, enriched with the following additional constraints:

$$x_j \in [\hat{x}_j^1 - \epsilon, \hat{x}_j^1 + \epsilon] \quad \forall j \in \{1, \dots, n_1\} \quad (19)$$

Value ϵ is a small constant given as an input parameter of the algorithm. Observe that our primal heuristic solves the problem only for the first NN, as preliminary experiments suggest that this is computationally more efficient. Finally, we explore the branch-and-bound tree by following a standard best-first strategy. Namely, we select the node with the largest upper bound on the objective value as the next node to be explored.

4.2.3 Updating Multipliers and Step Size

Phase Two relies on the identification of Lagrangian multipliers λ ; we start with $\lambda^0 = 0$ and some step size μ^0 . We update the values of the multipliers in each iteration using a standard

subgradient algorithm (Wolsey and Nemhauser 1999). Namely, at iteration $q \geq 1$, the subgradient algorithm solves (16) and records the optimal solution obtained as \bar{x}^q . The multipliers are then updated as

$$\lambda_{ij}^q = \lambda_{ij}^{q-1} - \mu^q (\bar{x}_j^{1q} - \bar{x}_j^{qi}) \quad \forall i \in \{2, \dots, e\}, j \in \{1, \dots, n_1\}. \quad (20)$$

Similarly, we update the step size in each iteration as follows:

$$\mu^q = \frac{\mu^{q-1}}{\sqrt{q}}. \quad (21)$$

We stop the subgradient algorithm after Q iterations. We then execute our Lagrangian relaxation-based branch-and-bound approach using the λ -multipliers obtained from the subgradient algorithm, and terminate once an optimal solution is found or a time limit is reached.

We remark that the subgradient procedure could be time consuming for large problem instances, as it requires solving Q MIPs given by Formulation (16). To accelerate these computations, we fix the values of the binary variables to be $z = \bar{z}$, where \bar{z} is part of the best feasible solution obtained in Phase One. With this, we can solve Formulation (16) as an LP, which allows to obtain reasonable initial values for the λ -multipliers quickly. Moreover, since formulation (16) is solved at every node of the branch-and-bound tree, we propose to keep updating the λ -multipliers and the step size according to (20) and (21) as we execute the branch-and-bound approach. Note that by doing this we (potentially) refine the quality of the λ -multipliers at the beginning of the exploration and since the step size value is reduced with every update, the change to the multipliers becomes negligible as the search explores deeper nodes in the branch-and-bound tree.

5 Computational Results

We present in this section the results of our computational experiments. In section 5.1 we describe the test problems used in our computations. In section 5.2, we compare the solution quality between single NN and NN ensemble using four benchmark functions with known optimal values. In section 5.3, we compare our approach with a state-of-the-art algorithm on the four benchmark functions mentioned above and two additional real-world datasets. Section 5.4 presents sensitivity analysis and additional experiments to assess the components of our two-phase approach.

We use Python 3.8, **Tensorflow** (Abadi et al. (2015)), and a 2.6 GHz 6-Core Intel i7-9750H CPU with 32 GB of RAM to train the neural networks of our data sets. We use Java implementations of **B&C** and **E-NN**, and we use Gurobi 9.0.2 to solve the mixed-integer programming formulations (Gurobi Optimization 2018). The experiments are executed on an Intel Xeon E5-1650 CPU (six cores) running at 3.60 GHz with 32 GB of RAM on Windows 10. Each execution is restricted by a time limit of 3,600 seconds. All code and instances are available upon request.

5.1 Test Problems

We use six data sets in our experiments. Four benchmark problems were extracted from the global optimization literature, and the other two are extracted from real-world applications that have been used in the Machine Learning and Optimization communities.

Peaks: The peaks function $f(x_1, x_2)$ is a benchmark instance in the global optimization literature (Schweidtmann and Mitsos (2019)). Peaks is defined over $[-3, 3]^2$ as

$$p(x_1, x_2) \equiv 3(1 - x_1^2)^2 e^{-x_1^2 - (x_2 + 1)^2} - 10 \left(\frac{x_1}{5} - x_1^3 - x_2^5 \right) e^{-x_1^2 - x_2^2} - \frac{e^{-(x_1 + 1)^2 - x_2^2}}{3}. \quad (22)$$

The goal is to identify a solution (x_1^*, x_2^*) such that $p(x_1^*, x_2^*)$ is minimum. The global optimal solution value is $p(\mathbf{x}^*) = -6.551$, which is attained at $x_1^* = 0.228$ and $x_2^* = -1.626$.

Beale: The Beale function is a continuous, non-differentiable, and multimodal function (Jamil and Yang (2013)) defined over $[-4.5, 4.5]^2$ and given by

$$b(x_1, x_2) \equiv (1.5 - x_1 + x_1x_2)^2 + (2.25 - x_1 + x_1x_2^2)^2 + (2.625 - x_1 + x_1x_2^3)^2 \quad (23)$$

The global minimum solution is $b(\mathbf{x}^*) = 0$, which is attained at $x_1^* = 3, x_2^* = 0.5$.

Perm: The Perm function is a parameterized function (Mishra (2006)). We consider the 3-dimensional version defined over $[-3, 4]^3$ as

$$m(x_1, x_2, x_3) \equiv \sum_{k=1}^3 \left\{ \sum_{j=1}^3 \left(j^k + \frac{1}{2} \right) \left[\left(\frac{x_j}{j} \right)^k - 1 \right] \right\}^2 \quad (24)$$

The global minimum is $m(\mathbf{x}^*) = 0$, which is attained at $\mathbf{x}^* = (1, 2, 3)$.

Spring: The Deflected Corrugated Spring function is another parameterized function (Mishra (2006)). We consider the 5-dimensional instance defined over $[0, 8]^4$ and given by

$$s(x_1, x_2, x_3, x_4, x_5) \equiv 0.1 \sum_{i=1}^5 (x_i - 4)^2 - \cos \left\{ 4 \sqrt{\sum_{i=1}^5 (x_i - 4)^2} \right\} \quad (25)$$

The global minimum solution is $s(\mathbf{x}^*) = -1$, which is attained at $\mathbf{x}^* = (4, 4, 4, 4, 4)$.

Wine: This first real-world application is based on the wine preference data set introduced by Cortez et al. (2009) (see also Mišić (2020)). In this work, the authors propose regression techniques to estimate the quality of a wine based on 11 features, such as the concentration of residual sugar and the relative volume of alcohol, using a data set with 1,599 samples. In the optimization version of the problem, we wish to identify the physicochemical properties of a wine that would have the highest quality.

Concrete: This second real-world application was introduced by Yeh (1998), who proposed the use of neural networks to predict the compressive strength of high-performance concrete based on 8 features, such as the densities of cement and water in the mixture, using 1,030 samples (see also Mišić (2020)). The optimization problem associated with **Concrete** can be interpreted as the identification of a concrete composition with maximum compressive strength.

Differently from **Beale**, **Spring**, **Perm**, and **Peaks**, optimal solutions for **Wine** and **Concrete** are unknown. Moreover, there is no simple (i.e., purely analytical) way of evaluating the quality of the solutions produced by our algorithms for these problems, as closed-formula expressions to evaluate the objective values are not available.

5.2 Comparison of Solution Quality

We experiment on synthetic datasets sampled from the instances for which we know optimal solutions: **Peaks**, **Beale**, **Perm**, and **Spring**. Specifically, we train a neural network on the sampled dataset to approximate the underlying function and then solve the optimization problem (1). The advantage of using benchmark functions for these experiments is two-fold:

1. We can calculate the true value of the optimal solution using a closed-form formula, and we also know the true global optimizer; and
2. Some benchmark functions resemble real-world problems with respect to the difficulty of training a good predictive model and finding the true global optimizer.

In the following section, we discuss how we create test instances for NNs/NN ensembles for optimization, and then provide a detailed comparison of the quality of the solutions using both methods.

5.2.1 Training and Optimization of Neural Networks

Generation of datasets. We generate $2000 + 1000 \times (n - 2)$ data points and calculate their respective objective values for each benchmark problem and each data set used for testing, where n is the number of dimensions. Thus, there are 2000, 2000, 3000, and 5000 data points for **Peaks**, **Beale**, **Perm**, and **Spring**, respectively. We adopt two sampling strategies to generate data sets; (a) *Latin Hypercube Sampling* (LHS) and (b) generating from a multivariate normal distribution, with mean given by the optimal solution and covariance matrix randomly drawn from the collection of symmetric positive-definite matrices (using `make_spd_matrix()` in the `sklearn` package). There are thus two data sets for each benchmark problem and therefore a total of eight data sets. For each data set we employ preprocessing to scale both the inputs and the output into range $[0, 1]$.

Model Selection `Tensorflow` (Abadi et al. 2015) is used to train the neural networks and a combination of `Tensorflow` and `BaggingRegressor` (Pedregosa et al. 2011) is used to train the NN ensembles. We utilize `RandomizedSearchCV` (Pedregosa et al. 2011) to conduct a hyper-parameter search of neural network models; specifically, we tune the number of hidden layers L , the number of neurons n in hidden layers, learning rate, the batch size, and the number of NNs e composing the ensemble; we use `Adam` optimizer for training and default settings in `Tensorflow` for other hyper parameters. For every data set, we conduct a search for a single NN and another one for an ensemble. Each search randomly samples 1000 combinations of hyper parameters and computes validation scores using K -fold cross validation. We then pick the four best combinations based on validation score. In the following sections, we let (e, L, n) represent a specific selected combination.

Training and Optimization of Instances For each configuration (e, L, n) , we randomly select 80% of the data set for training and use the remaining 20% as the test set. During training, we set aside 20% of the training set for Early Stopping to prevent over-fitting. We also log the Root Mean Squared Error (RMSE) on the test set. We finally solve the problem (1) with the trained model embedded and evaluate the quality of the solutions. The above training and optimization process is repeated to create 20 replications. Therefore, there are a total of 1280 experiment runs: 4 (four benchmark problems) \times 2 (two sampling strategies) \times 2 (single neural network and ensemble) \times 4 (four hyper parameter combinations) \times 20 (replicas). We set a 3,600 seconds time limit for optimization; for instances that cannot be solved to optimality within time limit, we use the best feasible solution found returned by the solver.

5.2.2 Analysis of Solution Quality

For instances trained on LHS sampled data sets, we evaluate the quality of the optimal solutions by calculating the actual function value of the optimal solutions and comparing it against the true global minimum. The results are shown in Figure 1, where each plot represents the results of a benchmark problem. On the horizontal axis, we report the configuration (e, L, n) atop the corresponding average test RMSE of 20 replications. The vertical axis represents the actual function value. Each boxplot shows the distribution of actual values of the 20 replicas for each configuration, with blue representing ensembles and orange representing single NNs. The red-dotted horizontal line is the true global minimum value. We also add a green interval to indicate the average actual values and its 95% confidence interval constructed by Bootstrapping.

One significant observation from Figure 1 is that the sizes, i.e., inter-quantile range (IQR), of the boxes associated with ensemble models are almost always smaller than that of single neural networks' across the benchmark problems, which suggests that the ensemble-based models is more stable. The lower variability resulting from using ensembles can also be observed by comparing the 95% confidence interval (CI) of the mean. Another observation is that the median and mean of the actual values obtained from optimizing with ensembles are closer to the true global minimum than when using single neural networks, i.e., the ensemble-based models

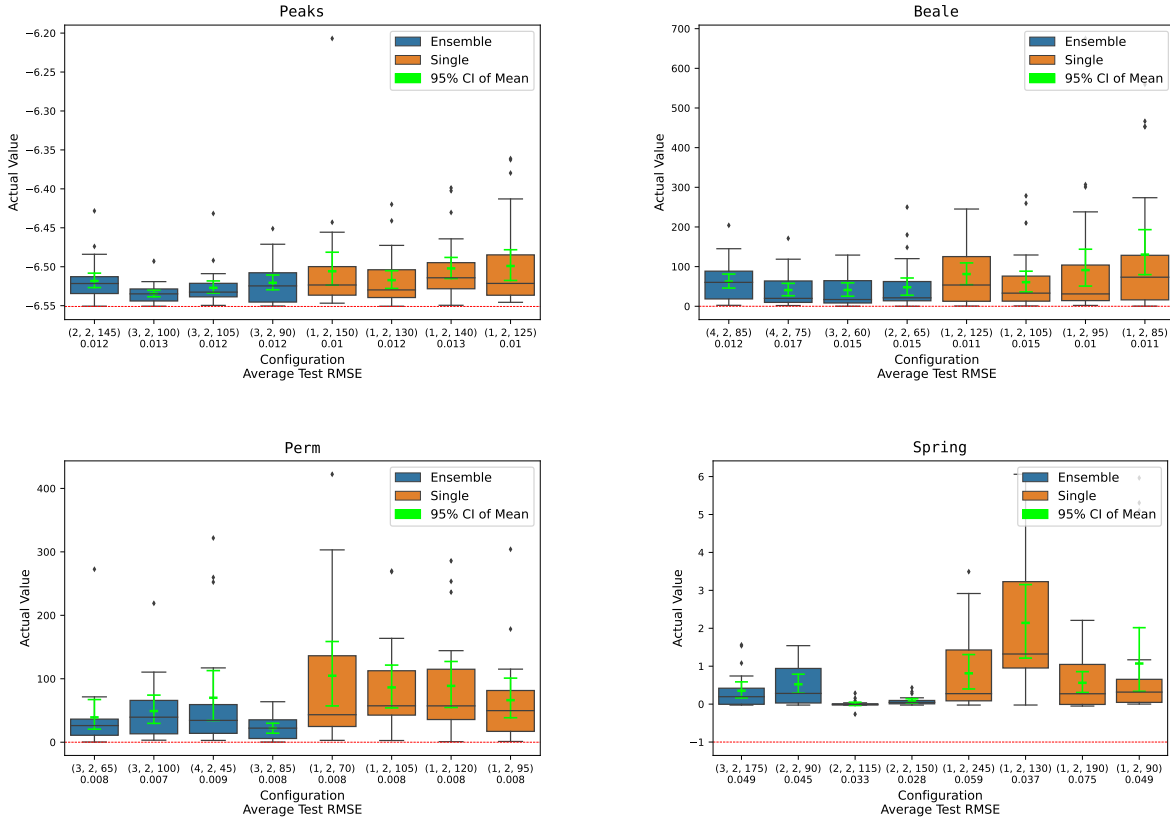


Figure 1: Distribution of Actual Values of Optimal Solutions and 95% Confidence Interval of the Mean

generate higher quality solutions. The average test RMSE between ensembles and single NNs are very close, thus ensuring a fair comparison.

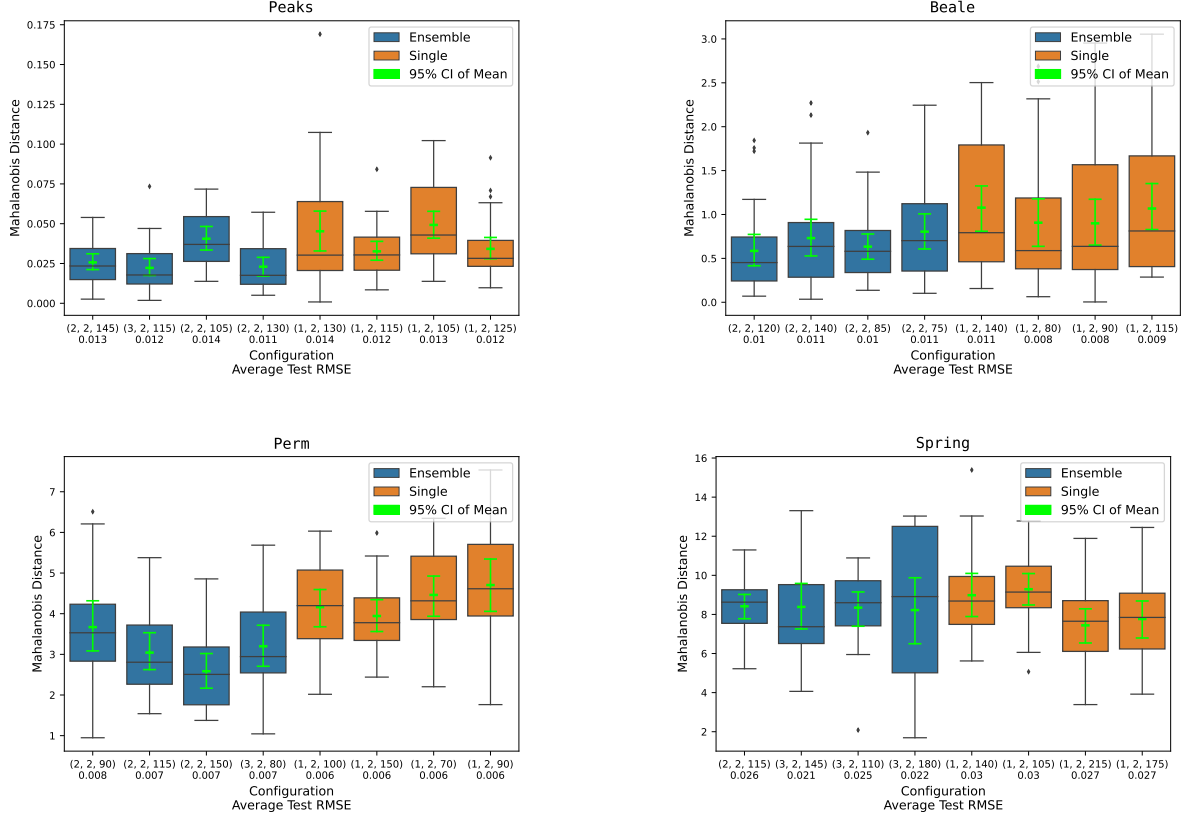


Figure 2: Distribution of Mahalanobis Distance and 95% Confidence Interval of the Mean

Of critical importance when using trained models with optimization frameworks is training relevance, i.e., the solutions obtained should be similar and ideally from the same distribution of the solutions used to train the models. For instances trained on data sets sampled from a multivariate normal distribution, we use the distance between the optimal solution and the points in the data set to measure the training relevance (Thebelt et al. 2021, Mistry et al. 2021); specifically, we use the *Mahalanobis distance*. The results are displayed in Figure 2 in boxplots similar to those in Figure 1, but with the vertical axis now representing the Mahalanobis distance. For **Peaks**, three out of four ensembles have lower median Mahalanobis distances than every single NNs' median value, and their 95% CI lie fully below the lower end of the first and third single NN's 95% CIs. For **Beale**, ensembles have smaller IQR and average Mahalanobis distance than single NNs. For **Perm**, all ensembles have a lower median than single NNs. For **Spring**, we see a mostly comparable collection of solutions, but one ensemble leads to a wide confidence interval. The above observation indicates that ensemble-based models generate solutions closer to historical data, and thus more reliable. Observe that we did not incorporate distance constraints in our methods to enforce these results.

We note here that for **Peaks**, **Beale**, and **Perm** we are reporting results identified by an implementation of model 4. For **Spring**, however, we are depicting the solutions obtained by our two-phase optimization model since it is a considerably harder problem.

5.3 Comparison with the State-of-the-Art Algorithm

5.3.1 Test Instances

We generate three random problem instances for each combination of $e \in \{3, 5\}$, $L \in \{2, 4\}$ and $n \in \{20, 40\}$, and for each of the six benchmark problems described above resulting in 144 instances. Observe that for $(5, 4, 40)$, the largest configuration, there are 800 neurons in the hidden layers controlled by a ReLU activation function, which in turns correspond to the number of auxiliary binary variables in the formulation.

5.3.2 Implementation details

We implement the state-of-the-art branch-and-cut approach **B&C** using callbacks, as described in [Anderson et al. \(2020\)](#). In preliminary computational experiments we found that imposing an upper limit on the total number of generated cuts helps to reduce the total computation time. We set this upper limit to 25,000 and compute the values for **LB** and **UB** by solving 2 LPs for each neuron.

Two-phase algorithm **E-NN** uses our proposed targeted strong bounds procedure to compute the values of **LB** and **UB**, and generates valid inequalities (10) via lazy cuts every time that a feasible integer solution is found. After fine tuning the parameters for **E-NN** on a subset of instances, we set $K = 1000$, $\tau = 0.01$, and a time limit of 5 seconds for the MILPs in the targeted strong bounding procedure. For the first phase we set a time limit of 180 seconds. For the second phase, we set the initial step size $\mu^0 = 0.05$, $Q = 20$, $\Delta = \epsilon = 0.02$. We set a time limit of 3,600 seconds for the entire optimization process (which includes the time spent in the first phase). The computational times reported in figures and tables include any time spent in pre-processing, computing bounds, separating cuts or valid inequalities, and finding λ -multipliers.

5.3.3 Performance of Optimization Algorithm

The performance of **B&C** and **E-NN** is summarized in Figures 3 and 4 and Table 1. Figure 3 shows a cumulative plot for **B&C** and **E-NN** in terms of execution time and optimality gap. Namely, on the left side of Figure 3, each point in a curve indicates the number of instances (y-axis) that were solved to optimality by the respective algorithm within the amount of time indicated in the x-axis. On the right side, the curves show the number of instances solved within the optimality gap indicated in the x-axis. We use log scale on both sides of the cumulative plot.

Figure 3 shows that the cumulative performance of **E-NN** is superior to that of **B&C**. Whereas both algorithms solve a significant number of instances within seconds, with a minor advantage of **B&C** on the easier ones, the performance of **B&C** clearly degrades on harder instances. These observations can be further investigated with the support of Table 1, which aggregates the results by problem, number e of ensembles, and number L of intermediate layers; these parameters are presented in the first three columns of the table. The table omits the number n of nodes per layer, and as we have three random instances per configuration, each entry aggregates the results of 6 instances. For each algorithm we report the average execution times (in seconds, with fractional values rounded up, and recording 3600 seconds for instances that reached the time limit), the number of instances solved to optimality, and the average gap of the instances that were not closed within 3,600 seconds.

The results presented in Table 1 show that our enhanced algorithm scales better than the baseline. Namely, **E-NN** solves more instances to optimality in all data sets and delivers considerably better gaps for instances with larger values of L and e . Observe that the relative performances of the algorithms are essentially equivalent across the different types of problem. For example, **Peaks** is one of the easiest problems; however, **B&C** could not solve any instances with 5 neural networks and 4 layers while **E-NN** solves all the instances within the time limit. The real-world problems are considerably harder; **Wine** is the most challenging problem, which can be explained by the number of input features. Whereas **E-NN** does deliver relatively high

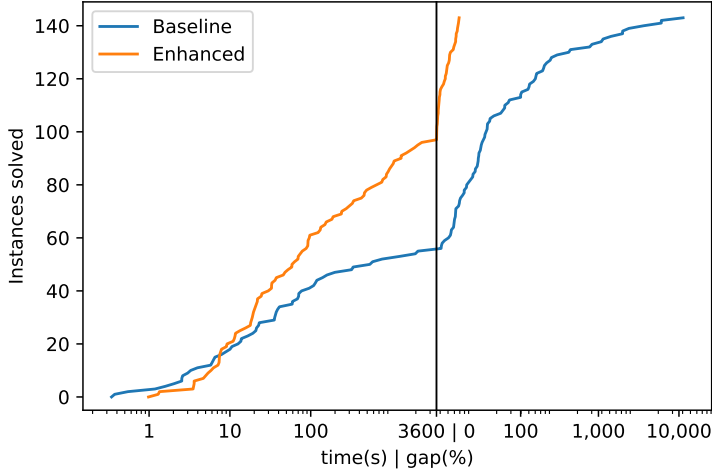


Figure 3: Cumulative performance plot comparing B&C and E-NN on all instances.

optimality gaps for some of the hardest instances, the plots in Figure 3 show that B&C can be orders of magnitude worse.

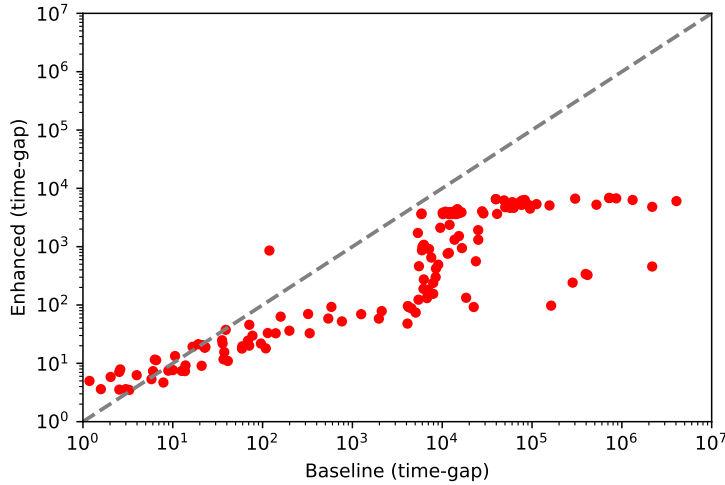


Figure 4: Scatter plot comparing execution time-gaps of B&C and E-NN on all instances.

Figure 4 is a scatter plot that compares the performance of B&C and E-NN. To account for differences in performance both in terms of time and gap, we present the results using *time-gap* as the metric describing the performance of each algorithm and on each instance. More precisely, the time-gap metric is given by the expression $t + 3,600 * \alpha$, where t is the time spent by the algorithm to solve the instance and α is the optimality gap achieved after 3,600 seconds. Observe that the time-gap metric reduces to the time t if the instance is solved within the time limit, and that t is capped at 3,600 otherwise. As in Figure 3, the results are presented in log scale. Although the results of the plot are affected by the multiplicative factor 3,600 applied to α , the differences in performance between the algorithms are clear. B&C is superior for some of the easier instances (those that could be solved within 5 minutes), but the rightmost part of

Table 1: Consolidated results

Instance			Baseline (B&C)			Enhanced (E-NN)		
Instance	e	L	Time	Solved	Gap	Time	Solved	Gap
Peaks	3	2	22	6	0	13	6	0
		4	1980	3	269	432	6	0
	5	2	98	6	0	34	6	0
		4	3600	0	293	755	6	0
Beale	3	2	6	6	0	4	6	0
		4	1814	3	4242	80	6	0
	5	2	16	6	0	12	6	0
		4	1889	3	27563	202	6	0
Perm	3	2	1024	5	41	36	6	0
		4	3353	1	177	1639	4	4
	5	2	1831	3	68	490	6	0
		4	3600	0	185	2028	3	4
Spring	3	2	1410	4	20	38	6	0
		4	3097	1	948	1886	3	41
	5	2	1820	3	116	110	6	0
		4	3600	0	3283	2046	3	44
Concrete	3	2	1820	3	166	1068	5	5
		4	3600	0	1022	3600	0	46
	5	2	3600	0	418	3006	2	2
		4	3600	0	1078	3600	0	48
Wine	3	2	1839	3	247	1954	3	10
		4	3600	0	26354	3600	0	44
	5	2	3600	0	1242	2655	2	29
		4	3600	0	21655	3600	0	62

the plot shows that E-NN largely outperforms B&C in harder instances (by orders of magnitude in some cases), for which the algorithms could not solve the problem to optimality.

We now analyze the execution time for the different stages of both algorithms for Beale, Spring, and Wine (complete results are presented in the Appendix A). Table 2 presents the results for B&C. We aggregate the three replicas associated with each configuration, given by the dataset, number of neural networks, number of layers, and number of nodes, which are presented in the first 4 columns. The last five columns report the results. The first indicates the number of replicas that were solved to optimality by B&C, whereas the other four columns report the average solution time (in seconds, capped at 3,600 for each experiment), optimality gap (as reported by Gurobi), pre-processing time, and time spent with the branch-and-cut algorithm, respectively. We note that the pre-processing time for B&C is a considerably small fraction of the total execution time across all instance configurations. All problems with 3 neural networks, 2 layers, and 20 nodes are solved in under 80 seconds; however, increasing the number of layers or the number of nodes has a dramatic effect on the performance of the algorithm. Instances not solved to optimality within the time limit exhibit exorbitant optimality gaps.

Table 3 shows the results of E-NN. The first eight columns are similar to their counterparts in Table 2. Columns “Phase 1” and “Phase 2” indicate the average time spent by E-NN in Phases 1 and 2, respectively. The last column shows the number of nodes explored in Phase 2. In contrast to B&C, pre-processing time for E-NN consumes a considerably larger fraction of the total execution time across all instance configurations, particularly for the harder ones. The easier instances are almost exclusively solved in Phase 1 while the harder instances are often solved in Phase 2. For the Wine instances, the amount of nodes explored within the time limit in the branch-and-bound tree of Phase 2 decreases for larger problems, which indicates that it takes considerably more time to explore a node. This result is expected as problem (16), solved at each node, becomes more computationally challenging as the number of networks, layers, or nodes increases. As mentioned above, the optimality gap for instances not solved within the time limit ranges on average between 2% and 89%, which is considerably better than the gaps for B&C.

Table 2: Computational Time Break Down for the Baseline algorithm

Instance	e	L	Nodes	Solved	Time	Gap (%)	Preprocess	B&B Time
Beale	3	2	20	3	1	0	0	0
			40	3	8	0	1	8
		4	20	3	29	0	1	27
			40	0	3600	4242	7	3593
	5	2	20	3	5	0	0	5
			40	3	27	0	2	25
		4	20	3	178	0	3	175
			40	0	3600	27563	19	3581
Spring	3	2	20	3	2	0	0	2
			40	1	2817	20	2	2816
		4	20	1	2595	106	2	2592
			40	0	3600	1508	20	3580
	5	2	20	3	40	0	1	39
			40	0	3600	116	4	3596
		4	20	0	3600	282	7	3593
			40	0	3600	6284	53	3547
Wine	3	2	20	3	78	0	0	78
			40	0	3600	247	2	3598
		4	20	0	3600	266	3	3597
			40	0	3600	52442	25	3575
	5	2	20	0	3600	103	1	3599
			40	0	3600	2382	6	3594
		4	20	0	3600	21991	8	3592
			40	0	3600	21320	45	3555

5.4 Evaluation of the Acceleration Strategies

We conduct additional computational experiments to understand the effects of our different model enhancements on the performance of the algorithm.

5.4.1 Experiments on Single Neural Networks

Since both the targeted bound procedure and the valid inequalities also work for single NNs, we compare them against other methods from the literature used for single NNs. For each problem class, we generate three random test instances with $e = 1$, $L \in \{2, 4\}$, and $n = 50$, for a total of 36 additional instances.

In our first set of experiments, we compare our targeted bound approach, denoted as TBP, with two other approaches. The first one computes the values of LB and UB by solving 2 LPs per neuron and is denoted by LP. The second approach computes LB and UB by solving 2 MILPs per neuron, with a time limit of 5 seconds per MILP, and is denoted by MILP. We design the following experiment to measure the performance of each method. We feed the values of LB and UB obtained by each of the methods to B&C and record the value of the bound obtained at the root node of the branch-and-bound tree. We also record the updated bound after adding 25,000 cuts of the type proposed by [Anderson et al. \(2020\)](#). We then compute the percent improvement of each of the bounds obtained with respect to the (weaker) bounds delivered by LP as follows:

$$\text{Percent bound improvement} = \frac{|\text{Bound} - \text{Bound LP}|}{|\text{Bound LP}|} \quad (26)$$

Table 4 presents the results for this experiment aggregated by problem class. Columns “Root” report the improvement over the root node bound obtained by LP and columns “Cuts” report the improvement to the bound after adding cuts. We also report the average time it takes to compute values for LB and UB in column “Time”, and the average number of MILPs solved in the pre-processing stage. The time used by LP is a fraction of the time used by MILP and TBP,

Table 3: Computational Time Break Down for the Enhanced algorithm.

Instance	e	L	Nodes	Solved	Time	Gap (%)	Preprocess	Phase 1	Phase 2	BB Nodes
Beale	3	2	20	3	1	0	1	0	0	0
			40	3	7	0	6	1	0	0
		4	20	3	16	0	12	5	0	0
			40	3	144	0	106	38	0	0
	5	2	20	3	5	0	4	0	0	0
			40	3	20	0	16	4	0	0
		4	20	3	29	0	24	4	0	0
			40	3	375	0	312	64	0	0
		3	20	3	7	0	6	1	0	0
			40	3	69	0	44	25	0	0
Spring	4	2	20	3	172	0	144	28	0	0
			40	0	3600	41	1198	180	2284	12
		5	20	3	18	0	13	5	0	0
			40	3	202	0	127	75	0	0
		4	20	3	492	0	446	45	0	0
			40	0	3600	44	2299	180	1203	6
	3	2	20	3	307	0	8	77	222	425
			40	0	3600	10	88	180	3377	82
		4	20	0	3600	12	288	180	3141	49
			40	0	3600	76	1576	180	1925	10
Wine	5	2	20	2	1711	2	22	180	1502	784
			40	0	3600	36	222	180	3262	35
		4	20	0	3600	36	826	180	2644	46
			40	0	3600	89	2792	180	722	3

Table 4: Computational Time Break Down for the Enhanced algorithm.

Instance	LP			MILP				TBP			
	Time	Root	Cuts	Time	Root	Cuts	MILPs	Time	Root	Cuts	MILPs
Beale	4	0%	78%	28	99%	100%	151	29	99%	100%	30
Peaks	6	0%	66%	108	80%	100%	151	103	78%	96%	54
Perm	7	0%	43%	196	68%	88%	151	139	66%	80%	58
Spring	6	0%	29%	453	74%	89%	151	241	68%	80%	62
Concrete	6	0%	17%	495	72%	72%	151	256	67%	67%	70
Wine	8	0%	23%	556	74%	74%	151	292	68%	68%	77
Average	6	0%	43%	306	78%	87%	151	177	74%	82%	59

as expected. The improvement to the bounds achieved by the cuts for LP is on average 43%. On the other hand, MILP exhibits the largest computational times and achieves an average bound improvement at the root node of 78% before adding cuts, and of 87% after adding the cuts, when compared to the bounds resulting from LP. Our approach achieves similar improvements of 74% at the root node and 82% after adding the cuts. Moreover, TBP uses considerably less computational time on average and solves fewer MILPs than MILP. We remark that depending on the definition of the critical neurons, controlled by parameter τ , TBP could mimic the behaviour of LP for large values of τ and the behaviour of MILP for small values of τ . We also note that the effect of the cuts is much more pronounced for LP, where the bounds after adding cuts are 43% better, whereas for the other methods the additional improvement obtained from the cuts is only 9% for MILP and 8% for TBP.

In the second set of experiments, we isolate the effect of the valid inequalities by comparing two approaches. We first compute the values of LB and UB by solving 2 LPs per neuron. Then, the first approach uses Formulation (4) without any valid inequalities or any other enhancements; we refer to this algorithm as **BigM**. The second approach includes valid inequalities (10) and is denoted as **BigM-VI**. We deactivate any preprocessing procedures and cuts from the solver for this experiment. We find that adding valid inequalities (10) when bounds are computed via LPs leads to a moderate increase in the average computational time while obtaining virtually the same optimality gap across all problem classes on single NNs. This suggest that valid inequalities

(10) are too loose to have a strong effect on the computational performance of the algorithm and that strategies to strengthen their coefficients are needed to make them more impactful. A table with the summary of these experiments is presented in the Appendix A.

5.4.2 Analyzing the Lagrangian Relaxation-Based Approach

We select a subset of 10 instances that are solved to optimality within the time limit during Phase Two and analyze some additional performance measures to better understand the behaviour of our proposed approach (3 instances for Peaks, 5 instances for Perm, and 2 instances for Concrete). Table 5 reports the results for this experiment. The first column reports the average total computational time. The second column reports the optimality gap obtained at the end of Phase One. The third column presents the gap obtained at the beginning of Phase Two, after running the subgradient algorithm. The fourth column reports the average number of times that the algorithm stops branching and reverts to the big-M formulation (which happens when the domain of the variables becomes too small). Column five shows the average depth of the nodes explored in the branch-and-bound tree of Phase Two, and the last column reports the average number of nodes explored.

Table 5: Analyzing the second phase of the algorithm.

Instance	Time	Gap 1	Gap 2	# BigM	Depth	Nodes
Peaks	1356	64%	1%	4	5	25
Perm	1198	9%	13%	47	12	1378
Concrete	1560	48%	20%	0	16	352
Average	1318	33%	11%	25	11	767

Table 5 shows that, on average, the bounds obtained after switching to Phase Two are considerably better than the bounds at the end of Phase One. This shows that the Lagrangian reformulation is on average tighter than the original formulation. There is an exception for instances of the **Perm** problem, in which the bounds at the end of Phase One are slightly better. This can be explained by the fact that, after terminating the MILP execution at the end of Phase One, we lose all the cuts and branching done by the solver up to that point.

We also find that the our algorithm reverts to the big-M formulation only for a relatively small fraction of the total number of nodes explored. In particular, this never happens for the **Concrete** instances, meaning that all the nodes are pruned by bounds before ever reverting to the big-M formulation. We also observe that the average depth of the nodes explored is at most 16, which is a direct consequence of following the best-first node selection strategy. Finally, the average time used by the subgradient algorithm is negligible (i.e., less than one second) for all the problem instances thanks to our strategy of fixing the binary variables and solving LPs instead of MILPs. On the contrary, when solving MILPs without fixing any variables, the computational times for the subgradient algorithm increases to several minutes in some cases.

6 Conclusion

Optimization models with embedded trained neural networks have been the focus of multiple studies from the literature in the past few years. We propose to use an ensemble of neural networks for optimization. Our experiments show that optimizing over ensembles delivers better and more robust results than optimizing over single NNs.

We propose a Two Phase algorithm to solve optimization problems with objective functions represented by ensembles of neural networks. We develop valid inequalities derived from a Benders decomposition approach and combine them with a targeted bound tightening procedure to reduce the computational times for the challenging optimization model at hand; these two techniques can also be applied to single NNs. Moreover, we explore the ensemble structure to develop a Lagrangian relaxation-based branch and bound algorithm, which is shown to improve

considerably over a direct formulation. Computational results show that our solution methods outperform an state-of-the-art branch-and-cut algorithm both in terms of CPU time and optimality gap, especially for large-sized ensembles of neural networks.

Our work opens different streams for future research. One direction relates to the interplay between the statistical properties of a trained neural network ensemble and its ensuing optimization model. We would like to investigate if predictors with lower MSE values directly result in optimization models with higher solution quality or which statistical performance measures of the predictors play a major role in ensuring that the optimization model produces high-quality solutions. Finally, we would like to explore alternative representations of the solution space which could result in tighter formulations (e.g., using decision diagrams to represent the space of feasible binary assignments of the auxiliary z -variables).

References

- Martín Abadi, Ashish Agarwal, Paul Barham, Eugene Brevdo, Zhifeng Chen, Craig Citro, Greg S. Corrado, Andy Davis, Jeffrey Dean, Matthieu Devin, Sanjay Ghemawat, Ian Goodfellow, Andrew Harp, Geoffrey Irving, Michael Isard, Yangqing Jia, Rafal Jozefowicz, Lukasz Kaiser, Manjunath Kudlur, Josh Levenberg, Dan Mané, Rajat Monga, Sherry Moore, Derek Murray, Chris Olah, Mike Schuster, Jonathon Shlens, Benoit Steiner, Ilya Sutskever, Kunal Talwar, Paul Tucker, Vincent Vanhoucke, Vijay Vasudevan, Fernanda Viégas, Oriol Vinyals, Pete Warden, Martin Wattenberg, Martin Wicke, Yuan Yu, and Xiaoqiang Zheng. TensorFlow: Large-scale machine learning on heterogeneous systems, 2015.
- Ross Anderson, Joey Huchette, Will Ma, Christian Tjandraatmadja, and Juan Pablo Vielma. Strong mixed-integer programming formulations for trained neural networks. *Mathematical Programming*, pages 1–37, 2020.
- Andrea Bartolini, Michele Lombardi, Michela Milano, and Luca Benini. Neuron constraints to model complex real-world problems. In *International Conference on Principles and Practice of Constraint Programming*, pages 115–129. Springer, 2011.
- J. F. Benders. Partitioning procedures for solving mixed variables programming problems. *Numerische Mathematik*, 4(1):238–252, 1962.
- David Bergman, Teng Huang, Philip Brooks, Andrea Lodi, and Arvind U Raghunathan. Janos: An integrated predictive and prescriptive modeling framework. *arXiv preprint arXiv:1911.09461*, 2019.
- Dimitris Bertsimas and Nathan Kallus. From predictive to prescriptive analytics. *Management Science*, 66(3):1025–1044, 2020.
- Dimitris Bertsimas, Allison O’Hair, Stephen Relyea, and John Silberholz. An analytics approach to designing combination chemotherapy regimens for cancer. *Management Science*, 62(5):1511–1531, 2016.
- Max Biggs, Rim Hariss, and Georgia Perakis. Optimizing objective functions determined from random forests. *Available at SSRN 2986630*, 2017.
- Max Biggs, Wei Sun, and Markus Ettl. Model distillation for revenue optimization: Interpretable personalized pricing. In *International Conference on Machine Learning*, pages 946–956. PMLR, 2021.
- Elena Botoeva, Panagiotis Kouvaros, Jan Kronqvist, Alessio Lomuscio, and Ruth Misener. Efficient Verification of ReLU-Based Neural Networks via Dependency Analysis. *Proceedings of the AAAI Conference on Artificial Intelligence*, 34(04):3291–3299, April 2020. ISSN 2374-3468, 2159-5399.
- Leo Breiman. Bagging predictors. *Machine learning*, 24(2):123–140, 1996.
- Rudy Bunel, Ilker Turkaslan, Philip H. S. Torr, Pushmeet Kohli, and M. Pawan Kumar. A

- Unified View of Piecewise Linear Neural Network Verification. *arXiv:1711.00455*, May 2018.
- Chih-Hong Cheng, Georg Nührenberg, and Harald Ruess. Maximum resilience of artificial neural networks. In *International Symposium on Automated Technology for Verification and Analysis*, pages 251–268. Springer, 2017.
- Paulo Cortez, António Cerdeira, Fernando Almeida, Telmo Matos, and José Reis. Modeling wine preferences by data mining from physicochemical properties. *Decision Support Systems*, 47(4):547–553, 2009.
- Thomas G. Dietterich. Ensemble methods in machine learning. *Lecture Notes in Computer Science (including subseries Lecture Notes in Artificial Intelligence and Lecture Notes in Bioinformatics)*, 1857 LNCS:1–15, 2000. ISSN 16113349. doi: 10.1007/3-540-45014-9_1.
- Souradeep Dutta, Susmit Jha, Sriram Sankaranarayanan, and Ashish Tiwari. Output range analysis for deep feedforward neural networks. In *NASA Formal Methods Symposium*, pages 121–138. Springer, 2018.
- Matteo Fischetti and Jason Jo. Deep neural networks and mixed integer linear optimization. *Constraints*, 23(3):296–309, 2018.
- Ian Goodfellow, Yoshua Bengio, and Aaron Courville. *Deep learning*. MIT press, 2016.
- Bjarne Grimstad and Henrik Andersson. ReLU networks as surrogate models in mixed-integer linear programs. *Computers & Chemical Engineering*, 131:106580, December 2019. ISSN 00981354.
- Inc. Gurobi Optimization. Gurobi optimizer reference manual, 2018. URL <http://www.gurobi.com>.
- Lars Kai Hansen and Peter Salamon. Neural network ensembles. *IEEE transactions on pattern analysis and machine intelligence*, 12(10):993–1001, 1990.
- Momin Jamil and Xin-She Yang. A literature survey of benchmark functions for global optimisation problems. *International Journal of Mathematical Modelling and Numerical Optimisation*, 4(2):150–194, 2013.
- Guy Katz, Clark Barrett, David L Dill, Kyle Julian, and Mykel J Kochenderfer. Reluplex: An efficient smt solver for verifying deep neural networks. In *International Conference on Computer Aided Verification*, pages 97–117. Springer, 2017.
- Hui Li, Xuesong Wang, and Shifei Ding. Research and development of neural network ensembles: a survey. *Artificial Intelligence Review*, 49(4):455–479, 2018.
- Sheng Liu, Long He, and Zuo-Jun Max Shen. On-Time Last-Mile Delivery: Order Assignment with Travel-Time Predictors. *Management Science*, November 2020. ISSN 0025-1909. doi: 10.1287/mnsc.2020.3741. URL <https://pubsonline.informs.org/doi/abs/10.1287/mnsc.2020.3741>.
- Michele Lombardi and Stefano Gualandi. A lagrangian propagator for artificial neural networks in constraint programming. *Constraints*, 21(4):435–462, 2016.
- Michele Lombardi, Michela Milano, and Andrea Bartolini. Empirical decision model learning. *Artificial Intelligence*, 244:343–367, March 2017. ISSN 00043702. doi: 10.1016/j.artint.2016.01.005. URL <https://linkinghub.elsevier.com/retrieve/pii/S0004370216000126>.
- Alessio Lomuscio and Lalit Maganti. An approach to reachability analysis for feed-forward ReLU neural networks. *arXiv:1706.07351 [cs]*, June 2017. URL <http://arxiv.org/abs/1706.07351>. arXiv: 1706.07351.
- Xiuyuan Lu and Benjamin Van Roy. Ensemble sampling. *Advances in neural information processing systems*, 30, 2017.
- Donato Maragno, Holly Wiberg, Dimitris Bertsimas, S. Ilker Birbil, Dick den Hertog, and Adejuyigbe Fajemisin. Mixed-Integer Optimization with Constraint Learning. *arXiv:2111.04469*, November 2021.

- Sudhanshu K Mishra. Global optimization by differential evolution and particle swarm methods: Evaluation on some benchmark functions. *Available at SSRN 933827*, 2006.
- Velibor V Mišić. Optimization of tree ensembles. *Operations Research*, 68(5):1605–1624, 2020.
- Miten Mistry, Dimitrios Letsios, Gerhard Krennrich, Robert M. Lee, and Ruth Misener. Mixed-Integer Convex Nonlinear Optimization with Gradient-Boosted Trees Embedded. *INFORMS Journal on Computing*, 33(3):1103–1119, July 2021. ISSN 1091-9856, 1526-5528. doi: 10.1287/ijoc.2020.0993. URL <http://pubsonline.informs.org/doi/10.1287/ijoc.2020.0993>.
- Fabian Pedregosa, Gaël Varoquaux, Alexandre Gramfort, Vincent Michel, Bertrand Thirion, Olivier Grisel, Mathieu Blondel, Peter Prettenhofer, Ron Weiss, Vincent Dubourg, et al. Scikit-learn: Machine learning in python. *Journal of machine Learning Research*, 12: 2825–2830, 2011.
- Artur M Schweidtmann and Alexander Mitsos. Deterministic global optimization with artificial neural networks embedded. *Journal of Optimization Theory and Applications*, 180(3): 925–948, 2019.
- Thiago Serra, Christian Tjandraatmadja, and Srikumar Ramalingam. Bounding and counting linear regions of deep neural networks. In *International Conference on Machine Learning*, pages 4558–4566. PMLR, 2018.
- Thiago Serra, Abhinav Kumar, and Srikumar Ramalingam. Lossless compression of deep neural networks. In *International Conference on Integration of Constraint Programming, Artificial Intelligence, and Operations Research*, pages 417–430. Springer, 2020.
- Chenbo Shi, Mohsen Emadikhiav, Leonardo Lozano, and David Bergman. Careful! training relevance is real. *arXiv preprint arXiv:2201.04429*, 2022.
- James E Smith and Robert L Winkler. The optimizer’s curse: Skepticism and postdecision surprise in decision analysis. *Management Science*, 52(3):311–322, 2006.
- Alexander Thebelt, Jan Kronqvist, Miten Mistry, Robert M Lee, Nathan Sudermann-Merx, and Ruth Misener. Entmoot: a framework for optimization over ensemble tree models. *Computers & Chemical Engineering*, 151:107343, 2021.
- Vincent Tjeng, Kai Xiao, and Russ Tedrake. Evaluating Robustness of Neural Networks with Mixed Integer Programming. *arXiv:1711.07356*, February 2019. arXiv: 1711.07356.
- Calvin Tsay, Jan Kronqvist, Alexander Thebelt, and Ruth Misener. Partition-based formulations for mixed-integer optimization of trained relu neural networks. *arXiv preprint arXiv:2102.04373*, 2021.
- Sicco Verwer, Yingqian Zhang, and Qing Chuan Ye. Auction optimization using regression trees and linear models as integer programs. *Artificial Intelligence*, 244:368–395, 2017.
- Juan Pablo Vielma. Mixed Integer Linear Programming Formulation Techniques. *SIAM Review*, 57(1):3–57, January 2015. ISSN 0036-1445, 1095-7200. doi: 10.1137/130915303. URL <http://epubs.siam.org/doi/10.1137/130915303>.
- Keliang Wang, Leonardo Lozano, David Bergman, and Carlos Cardonha. A two-stage exact algorithm for optimization of neural network ensemble. In *International Conference on Integration of Constraint Programming, Artificial Intelligence, and Operations Research*, pages 106–114. Springer, 2021.
- Segev Wasserkrug, Orit Davidovich, Evgeny Shindin, Dharmashankar Subramanian, Parikshit Ram, Pavankumar Murali, Dzung Phan, Nianjun Zhou, and Lam M Nguyen. Ensuring the quality of optimization solutions in data generated optimization models. In *The 30th International Joint Conference on Artificial Intelligence (IJCAI 2021)*, 2022.
- Laurence A Wolsey and George L Nemhauser. *Integer and combinatorial optimization*, volume 55, page Page 46. John Wiley & Sons, 1999.
- Kai Y. Xiao, Vincent Tjeng, Nur Muhammad Shafiullah, and Aleksander Madry. Training for Faster Adversarial Robustness Verification via Inducing ReLU Stability. *arXiv:1809.03008*, April 2019.

- I-C Yeh. Modeling of strength of high-performance concrete using artificial neural networks. *Cement and Concrete research*, 28(12):1797–1808, 1998.
- Zhi-Hua Zhou, Jianxin Wu, and Wei Tang. Ensembling neural networks: many could be better than all. *Artificial intelligence*, 137(1-2):239–263, 2002.

A Detailed results

We show the complete results of our numerical experiments in Tables 6 – 8. All entries associated with time are reported in seconds, and the optimality gaps are the percentage values reported by Gurobi. Average values are rounded to the closest integer value. Table 6 extends Table 2 (with all the results of B&C), and Table 7 extends Table 3 (for E-NN); the columns in both tables are similar to their counterparts in the main text. Finally, Table 8 reports the results for the sensitivity analysis on the effect of the valid inequalities; in addition to the number of instances solved, the average solution time, and the average gap for each algorithm, we report the average number of cuts generated by BigM-VI.

Table 6: Results for Baseline algorithm.

Instance	e	L	Nodes	Solved	Time	Gap	Preprocess	B&B Time
Beale	3	2	20	3	1	0	0	0
			40	3	8	0	1	8
			20	3	29	0	1	27
		4	40	0	3600	4242	7	3593
			20	3	5	0	0	5
			40	3	27	0	2	25
	5	2	20	3	178	0	3	175
			40	0	3600	27563	19	3581
			20	3	39	0	0	39
		4	40	0	3600	166	2	3598
			20	0	3600	237	3	3597
			40	0	3600	1808	24	3576
Concrete	3	2	20	0	3600	59	1	3599
			40	0	3600	777	5	3595
			20	0	3600	800	8	3592
		4	40	0	3600	1355	66	3534
			20	3	3	0	0	3
			40	3	42	0	1	40
	5	2	20	3	359	0	2	357
			40	0	3600	269	15	3585
			20	3	13	0	1	12
		4	40	3	184	0	4	180
			20	0	3600	184	6	3595
			40	0	3600	403	37	3563
Perm	3	2	20	3	10	0	0	10
			40	2	2037	41	2	2035
			20	1	3107	16	2	3105
		4	40	0	3600	284	15	3585
			20	3	62	0	1	61
			40	0	3600	68	4	3596
	5	2	20	0	3600	81	5	3595
			40	0	3600	289	41	3559
			20	3	2	0	0	2
		4	40	1	2817	20	2	2816
			20	1	2595	106	2	2592
			40	0	3600	1508	20	3580
Spring	3	2	20	3	40	0	1	39
			40	0	3600	116	4	3596
			20	0	3600	282	7	3593
		4	40	0	3600	6284	53	3547
			20	3	78	0	0	78
			40	0	3600	247	2	3598
	5	2	20	0	3600	266	3	3597
			40	0	3600	52442	25	3575
			20	0	3600	103	1	3599
		4	40	0	3600	2382	6	3594
			20	0	3600	21991	8	3592
			40	0	3600	21320	45	3555
Wine	3	2	20	3	78	0	0	78
			40	0	3600	247	2	3598
			20	0	3600	266	3	3597
		4	40	0	3600	52442	25	3575
			20	0	3600	103	1	3599
			40	0	3600	2382	6	3594
	5	2	20	0	3600	21991	8	3592
			40	0	3600	21320	45	3555
			20	0	3600	103	1	3599
		4	40	0	3600	2382	6	3594
			20	0	3600	21991	8	3592
			40	0	3600	21320	45	3555

Table 7: Results for Enhanced algorithm.

Instance	e	L	Nodes	Solved	Time	Gap	Preprocess	Phase 1	Phase 2	BB Nodes
Beale	3	2	20	3	1	0	1	0	0	0
			40	3	7	0	6	1	0	0
			40	3	16	0	12	5	0	0
	5	2	20	3	144	0	106	38	0	0
			40	3	5	0	4	0	0	0
			40	3	20	0	16	4	0	0
Concrete	3	2	20	3	29	0	24	4	0	0
			40	3	375	0	312	64	0	0
			40	3	18	0	6	12	0	0
	5	2	20	2	2117	2	67	180	1865	367
			40	0	3600	5	291	180	3118	220
			40	0	3600	71	1477	180	1985	10
Peaks	3	2	20	1	2971	1	16	180	2762	12787
			40	1	3040	1	148	180	2698	334
			40	0	3600	16	780	180	2632	125
	5	2	20	0	3600	79	2681	180	842	4
			40	3	4	0	3	0	0	0
			40	3	22	0	16	6	0	0
Perm	3	2	20	3	40	0	35	5	0	0
			40	3	824	0	505	180	139	19
			40	3	7	0	7	1	0	0
	5	2	20	3	60	0	44	16	0	0
			40	3	129	0	106	23	0	0
			40	3	1381	0	979	180	221	25
Spring	3	2	20	3	7	0	3	4	0	0
			40	3	64	0	21	43	0	0
			40	3	89	0	37	52	0	0
	5	2	20	1	3189	1	832	180	2192	150
			40	3	14	0	7	6	0	0
			40	3	966	0	70	180	716	1863
Wine	3	2	20	3	457	0	110	150	196	357
			40	0	3600	4	1608	180	1795	66
			40	3	7	0	6	1	0	0
	5	2	20	3	69	0	44	25	0	0
			40	3	172	0	144	28	0	0
			40	0	3600	41	1198	180	2284	12

Table 8: Assessing the effect of the valid inequalities.

Instance	BigM			BigM-VI			
	Solved	Time	Gap	Solved	Time	Gap	# Cuts
Beale	6	17	0%	6	17	0%	5
Peaks	3	1868	85%	3	1858	86%	13
Perm	6	453	0%	6	804	0%	7
Spring	3	1803	21%	3	1803	21%	9
Concrete	3	1802	39%	3	1802	38%	7
Wine	3	2379	96%	3	2465	96%	15
Average	24	1387	40%	24	1458	40%	9

B Details of the Hyper Parameters Configuration

Table 9 reports the hyper parameters of the selected configurations (see Section 5.2). The LHS columns contain NNs trained on latin hypercube sampled dataset, whereas the MVN columns contain NNs trained on data set sampled from multivariate normal distribution. Observe that $e = 1$ represents single NNs, whereas $e > 1$ represents ensembles.

Table 9: Hyper parameters of selected configurations

Instance	LHS					MVN				
	e	L	Nodes	Learning Rate	Batch Size	e	L	Nodes	Learning Rate	Batch Size
Peaks	2	2	145	0.0008035	32	2	2	145	0.0011023	32
	3	2	105	0.0009381	32	3	2	115	0.0009605	32
	3	2	90	0.0016427	32	2	2	105	0.0011276	32
	3	2	100	0.0007235	32	2	2	130	0.0009183	32
	1	2	140	0.0020914	32	1	2	130	0.0021041	32
	1	2	150	0.0005355	32	1	2	115	0.0011318	32
	1	2	130	0.0014449	32	1	2	105	0.0015904	32
	1	2	125	0.0007010	32	1	2	125	0.0009507	32
Beale	4	2	85	0.0008707	32	2	2	120	0.0016596	32
	2	2	65	0.0010586	32	2	2	140	0.0019661	32
	3	2	60	0.0021587	64	2	2	85	0.0017663	32
	4	2	75	0.0022218	32	2	2	75	0.0019195	32
	1	2	105	0.0020312	64	1	2	140	0.0026932	32
	1	2	85	0.0004390	32	1	2	80	0.0037704	32
	1	2	125	0.0003647	64	1	2	90	0.0020293	32
	1	2	95	0.0004334	64	1	2	115	0.0025659	32
Perm	3	2	65	0.0005243	32	2	2	90	0.0003264	64
	3	2	100	0.0004778	64	2	2	115	0.0004152	32
	4	2	45	0.0007861	32	2	2	150	0.0003464	64
	3	2	85	0.0007125	32	3	2	80	0.0006148	64
	1	2	70	0.0007341	32	1	2	100	0.0001573	32
	1	2	105	0.0005455	64	1	2	150	0.0003580	32
	1	2	120	0.0004419	64	1	2	70	0.0003460	32
	1	2	95	0.0005871	32	1	2	90	0.0003411	32
Spring	3	2	175	0.0052601	32	2	2	115	0.0021206	32
	2	2	90	0.0016923	32	3	2	145	0.0015516	32
	2	2	115	0.0021206	32	3	2	110	0.0023950	32
	2	2	150	0.0019307	32	3	2	180	0.0021299	32
	1	2	245	0.0032445	32	1	2	140	0.0017628	32
	1	2	130	0.0016556	32	1	2	105	0.0016161	32
	1	2	190	0.0035503	32	1	2	215	0.0014401	32
	1	2	90	0.0022293	32	1	2	175	0.0015953	32